2021 IEEE 12th International Symposium on Power Electronics for Distributed Generation Systems (PEDG) | 978-1-6654-0465-5/21/$31.00 ©2021 IEEE | DOI: 10.1109/PEDG51384.2021.9494251

An Optimal Design of a Hybrid Liquid/Air Cooling System for High Power, Medium Frequency, and Medium Voltage Solid-State Transformer

Siavash Beheshtaein[1], Ahmad Alshafei[1], Garry Jean-Pierre[1], Necmi Altin[2], Mahydy Khayamy[1], Robert Cuzner[1], and Adel Nasiri[1]
[1]University of Wisconsin Milwaukee, Milwaukee, USA
[2]Department of Electrical & Electronics Engineering, Faculty of Technology, Gazi University, Ankara, Turkey
beheshta@uwm.edu, aie@uwm.edu, jeanpie4@uwm.edu, naltin@gazi.edu.tr, mkhayamy@uwm.edu, cuzner@uwm.edu, nasiri@uwm.edu

***Abstract*— In this paper, a 10 kV SiC MOSFET-based solid-state transformer (SST) operating at 13 kV to 7.2 kV, 667 kW, and 20 kHz is modeled and optimized to reach maximum power density and efficiency. In order to reach optimum configuration, different core material/type/size, primary/secondary turns, insulation type/thickness, and cooling systems are considered; then based on a systematic approach the best solution is obtained. To reach this goal, the magnetic part of SST forced air-cooling, and the water-cooling system is modeled in ANSYS MAXWELL/Simplorer, ANSYS-ICEPAK, and ANSYS-FLUENT, respectively. The simulation results show a high efficient SST with an effectiveness of the cooling system.**

Index Terms*— *10 kV SiC MOSFETs, liquid cooling, isolated dc/dc, High-power density, medium voltage (MV), MV transformer.

I. INTRODUCTION

Recently, several research studies have been conducted in Solid-State Transformer (SST) is one of the main promising technology in developing a high-efficient and compact power conversion system from medium voltage (MV) utility grid to chip voltage level in the data center [1]. This technology is a combination of the power converters and medium (or high) frequency transformer that can provide a more compact and efficient solution with improved control and monitoring functions. What are needed as enablers for high power systems are MV interfacing SSTs that have sufficient power throughput for multi-MW systems. Since the transformer is the biggest component of the SST, the system must operate in frequency to reach compactness. Therefore, in order to reach high compact SST, an optimum MV Medium Frequency (MVMF) Transformer must be designed.

The majority of MV SST implementations are based upon the connection of lower voltage rated modular isolated converters in series to divide the total system voltage stress across these modular converters. On the other hand, with the advance in wide-bandgap devices, high power dense, high frequency, and high voltage modules

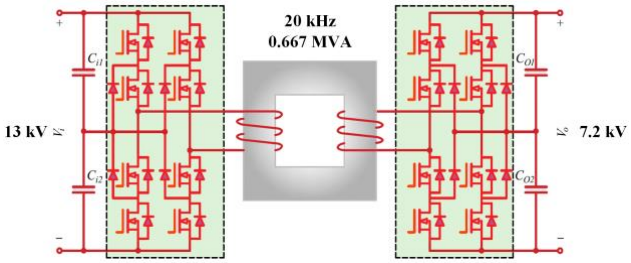

Fig. 1. The simulated NPC-NPC SST.

such as 10 kV Silicon Carbide (SiC) MOSFET, are developed by CREE/WOLFSPEED [2] and Virginia Tech [3], MVMF SST can reach higher power density and efficiency.

In MV SST, the switches in the two-level dual active bridge (DAB) need to withstand the whole dc-link voltage. For medium or high power voltage applications DAB can not be used, and other dc-dc isolated dc-dc converters including cascaded two-level DAB converter [4],[5], advanced power device [6],[7], multilevel converter [8], and neutral point clamped (NPC) [9],[10] must be considered. One of the most promising topologies for the MVMF-SST is NPC DAB. The voltage stress in this topology is decreased to the half of voltage under the dual-phase-shifted (DPS) modulation [10]. In addition, it can enhance control flexibility and proper regulation of the transmission power.

Although operating in MVMF will results in high power density, high power loss density especially in transformer brings up many challenges. Isolated MVMF dc/dc is the transformer that is responsible for voltage step down and the galvanic isolation between two MV sides. Although low-frequency transformer works under sinusoidal voltage with grid frequency, the MVMF transformer operates with square voltages and nonsinusoidal current with MF. This has an adverse effect on the core and winding losses, insulation coordination, cooling system, and electrical parameter control [11].

978-1-6654-0465-5/21/$31.00 ©2021 IEEE

TABLE I. TABLE TYPE STYLES MAGNETIC MATERIAL PROPERTIES

Core material	Flux density (T)	Specific loss (kW/kg)	Permeability	Frequency (kHz)	Cost ($/kg)
Silicon steel	1.8	0.2	1000-3000	<1	14,5
Amorphous	1.56	0.2-1	2000-200000	<500	19.5
Ferrite	0.45	0.009	1500-10000	20-200	6.5
Nanocrystaline	1.2	0.01-0.14	1800-200000	<500	28

While transformer isolation is easily achieved for low voltage and high-frequency or high-voltage and low-frequency, it is a challenging issue for MVMF transformers. On the medium voltage side, the insulation layer thickness that encapsulates MV-winding from the other MV-winding or core must be large enough to provide adequate dielectric strength. The winding power and core losses flow through the insulation layer, which has low thermal insulation, results in a hot spot in the insulation layer. The transformer compactness can affect transformer temperature and therefore for a highly compact transformer, an advanced cooling system is required. In addition, proper selection of the insulation material is important, because, for MVMF transformer dielectric loss is considerable and causes local hot spots [12]. Generally, the MVMF transformer is designed based on discrete optimization problems with objectives such as minimizing size, minimizing power loss. Analytical [13],[14], and numerical [15]–[18] are two main approaches for solving the optimization problem. Numerical solution employes computer software program to solve the problem. This type is solution can be used for complicated design, however, there is no general rule for transformer design. On the other hand, the analytical method solves the problem based on a closed-form formula and reaches results quickly. The main disadvantage is that closed formulation is not easy to obtain. In addition, due to simplification, this approach does not give accurate results.

This paper proposed and designed a 13.8 kVAC and 4.16 kVAC (three-level to three-level) SST with a single-phase power at 667 kVA for a 2MVA three-phase system (see Fig. 1). The primary and secondary converters are designed with 10 kV SiC MOSFET to reach higher power density and efficiency. Based on the assumed power rating, input/output voltages, and currents, an MVMF is designed. Finally, a forced air-cooling system is designed for the MVMF in ANSYS-ICEPAK. Similarly, based on the current amplitude in each module, the conducting and switching power losses are calculated. Finally, a water cooling system is designed in ANSYS-FLUENT.

II. SYSTEM DESIGN

The main purpose of designing a power conversion system is to increase power density and efficiency. As the frequency increases, the size of the electrical component decreases, however increasing the frequency has an adverse effect on the core loss, switching loss, and reduce efficiency. On the other hand, regarding a fixed rating power, choosing a higher voltage rating results in a decreasing power rating and improving efficiency. One of the main obstacles in choosing a higher voltage is the ability to manage the electric field as well as electric flux density.

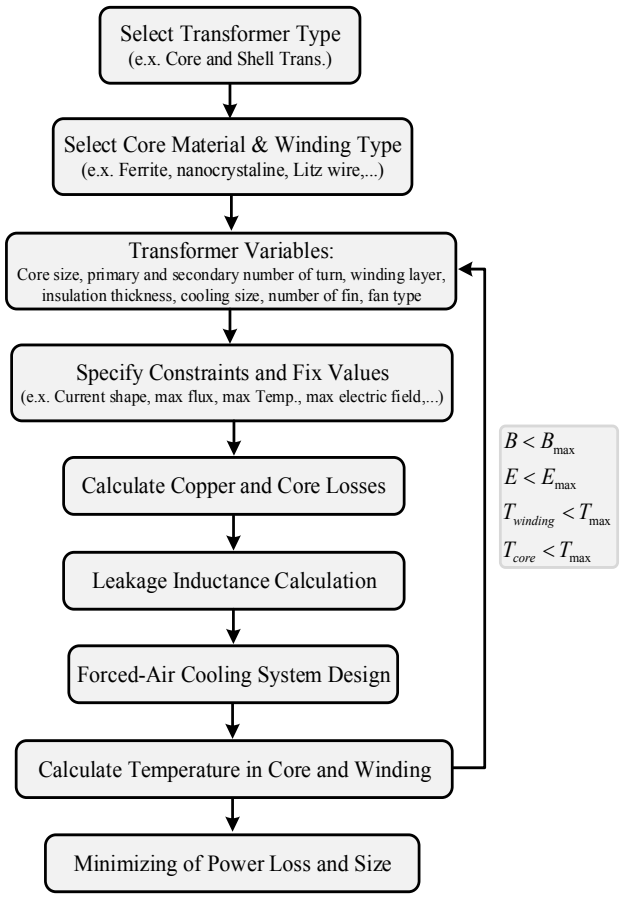

Fig. 2. Proposed process for MFMV transformer design.

Regarding all these facts, it is critical to design and optimize both SST as well as primary and secondary converters. As shown in Fig. 2, in the first step, different transformer types including coaxial, core, and shell types are considered then the best one is selected according to the application. Regarding all these facts, it is critical to design and optimize both SST as well as primary and secondary converters.

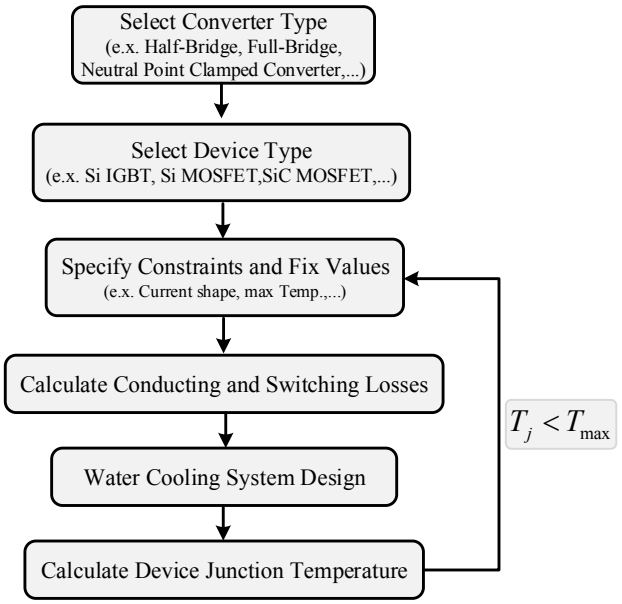

Fig. 3. Proposed process for converter design.

As shown in Fig. 2, in the first step, different transformer types including coaxial, core, and shell types are considered then the best one is selected according to the application. In step2, core (i.x. Ferrite, nanocrystalline, amorphous,…) and winding material (i.e. litz, foil, roll cable) is selected according to cost, maximum flux density, and core loss. In step 3, different transformer variables including core dimension, number of the primary and secondary winding turn, number of the primary and secondary winding layer, insulation thickness, heatsink size, number of heatsink fin, and fan type are selected. In step 4, different constraints such as maximum core flux density, maximum winding/core temperature, current shape, maximum electric field are applied. In steps 5-7, transformer loss, leakage inductance, the temperature in core/winding are calculated. Then, this process continues for a specific number of iterations. Finally, appropriate properties of transformer variable, as well as forced air-cooled system dimension that results in the highest efficiency and compactness, are obtained.

For the converter part (as shown in Fig. 3), first, among converter types such as half-bridge, full-bridge, Neutral Point Clamped (NPC) converter, NPC converter is chosen. Then, in step 2, among different device types including Si IGBT, Si MOSFET, and SiC MOSFET, 10 kV SiC MOSFET is selected according to demanded efficiency and cost. In step 3, different constraints such as maximum junction temperature, efficiency, current shape are applied. Then, switching and conducting losses are calculated, and based on that, the temperature distribution in the converter part is estimated. In the last step, a water-cooled system is designed in such a way to limit the maximum junction temperature below its allowed value.

III. Transformer Design

A. Area product

The area product is a product of the core and wind cross-sections. The core area product is important for having a high dense SST. This can be formulated as:

$$A_p = A_c A_w \approx \frac{P_n}{k_f k_u B_m J_m f_{sw}} \tag{1}$$

where A_c, A_w, P_n, k_f, k_u, B_m,, J_m, and f_{sw} are core cross-section, core window area, operating power, waveform coefficient, core window utilization, peak flux density, current density, and switching frequency, respectively. P_n, k_f, k_u, B_m, J_m, and f_{sw} are limited by the specific application, defined by converter waveform, limited by transformer construction, limited by material characteristics, and limited by thermal characteristics, and switch capability. According to this formula, to decrease density switching frequency must be increased. However, power loss and thermal issues are two main limitations for increasing the frequency.

B. Transformer core material and type

As shown in Fig. 2, the first step for designing SST is the selection of material as well as core type. Different materials can be used for shaping the transformer core. Among them, silicon steel, for the 667 MW/20 kHz system, different amorphous, ferrite, and nanocrystalline are more practical. In order to pick up an appropriate material, characteristics including flux density, power loss, permeability, frequency, and cost must be considered. Table I shows a comparison of the core material based on the above-mentioned attribute.

As can be seen, the most appropriate material for the 667 MW/20 kHz system is the one operating in this range and has the lowest loss and power loss. Therefore, ferrite is selected. Shell and core structures are two MFMV transformers. The core type transformer composes of one magnetic core with two windings around the core limbs. However, in shell-type two primary and secondary windings are wound on the middle limb, and two other limbs are connected to the middle limb. It has been shown that the shell-type transformer has a higher power density for the same efficiency. In addition, the core temperature in a shell-type is lower than a core-type transformer. The leakage inductor of shell-type is slightly lower than the core type. However, because of the magnetic field trajectory flow in the core, the leakage can be controlled easier [19]. Therefore, the shell-type transformer is selected for the 667 MW/20 kHz system.

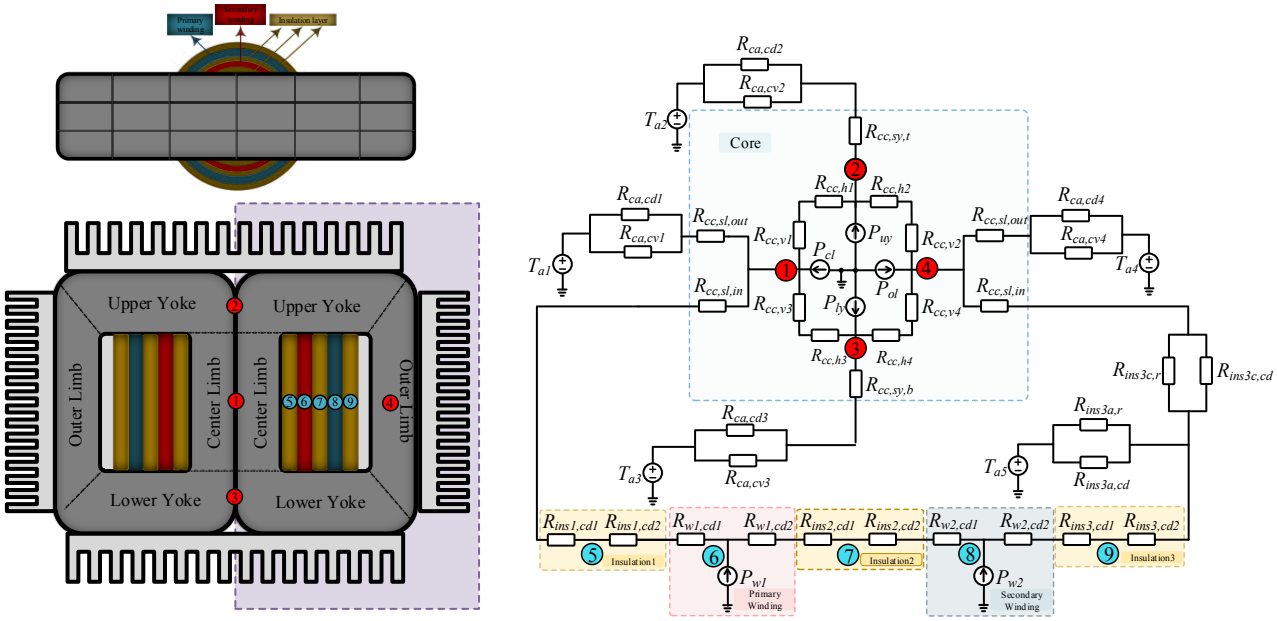

(a) (b)

Fig. 4. (a) 2-D MVMF transformer with nodal temperature locations. (b) Thermal network modeling of the highlighted part of the MVMF transformer with conduction, convection, and radiation thermal resistances.

C. Core loss

Core loss includes hysteresis, eddy, and residual losses. Core loss depends on magnetization, flux density magnitude, and operating frequency, and core material. Core loss can be calculated by the Steinmetz formula. Steinmetz formula gives simple and satisfactory accuracy. The core loss expression by Steinmetz is as:

$$P_{core} = K.V_c.f^{\alpha}.B_m^{\beta} \tag{2}$$

where K, α, and β are material coefficients that can be obtained from the manufacturer datasheet by applying curve fitting. V_c is the magnetic core volume in a cubic centimeter. Since the material core is ferrite the K, α, and β, are 42.8, 1,53, and 2.98, respectively [20].

D. Winding loss

Winding loss is the summation of both dc and ac losses. In the low-frequency system, ac loss can be neglected. However, for medium and high-frequency transformers, eddy current loss, which is due to skin and proximity effects, is considerable. According to Dowell's equation, ac resistance is the summation of resistance generated from the skin (4) and proximity effects (5)

$$\zeta = h/\sigma \tag{3}$$

$$R_{ac,skin} = \frac{\xi}{2}.\frac{\sinh(\xi)+\sin(\xi)}{\cosh(\xi)-\cos(\xi)}.R_{dc} \tag{4}$$

$$R_{ac,proximity} = \frac{\xi}{2}.(2m-1)^2.\frac{\sinh(\xi)-\sin(\xi)}{\cosh(\xi)+\cos(\xi)}.R_{dc} \tag{5}$$

where ζ, h, and σ are penetration ratio, wire thickness, and skin depth, respectively. And the magnitude of m corresponds to the MMF of each layer [21]. Regarding the calculated R_{ac}, the winding power loss of non-sinusoidal current waveform is obtained as:

$$P_{winding} = \sum_{n=1}^{n} R_{ac}(n) I_{RMS}(n)^2 \tag{6}$$

E. Cooling system design

Calculating the MFMV transformer hot spot is a complicated heat transfer problem. Regarding the transformer symmetric, the 3D heat transfer model can be simplified to a 2D model. The core area is divided into four zones including center limb, outer limb, upper yoke, and lower yoke. The core loss is assumed to be evenly distributed within the core volume. Therefore, the injected power loss in each core zone is proportional to its volume with respect to the total core loss. Each insulator layer, primary and secondary windings are represented by a separated zone. Thermal coupling between all of the zones is also considered, In addition, conduction, convection, and radiation thermal networks are used to thermally connect two closed surfaces or a surface to the ambient air connect the solid surface. Regarding the above-mentioned consideration, the total thermal network of the MFMV transformer (see Fig.4 (a)) is shown in Fig.4 (b). The temperatures at all nodes can be calculated based on the inversion of the admittance matrix of the thermal network and injected power losses as follows:

$$\Delta T = Y^{-1} P_{loss} \tag{7}$$

According to (7), a proper cooling system must be designed in such a way to do not to let the calculated temperature exceed a specified maximum allowed value.

When an MFMV transformer is built based on complicated structures and multiple materials, the thermal network modeling can be a sophisticated problem. Finite element analysis (FEA) is an effective tool for obtaining temperatures at different locations inside the component with high precision. Therefore, this method is taken into account for designing a forced-air cooling system.

IV. Converter Design

In this study, an MV SST is designed to interface between 13.8 kVAC and 4.16 kVAC with a single-phase power at 667kVA for a 2MVA three-phase system. The primary-side inverter is designed with 10 kV SiC MOSFET that can handle a 13kV DC bus in a three-level topology. Since 10 kV SiC MOSFET is used for the secondary side, a 2-level inverter topology is an appropriate candidate.

A. 10 kV MOSFET packaging

The switches in the primary and secondary sides are needed to be selected based on the SST specification and topology. On the primary side, the voltage stress on the switch is equal to half a dc-link, which is 6.5 kV. On the other hand, the voltage stress on the switch on the secondary side is equal to the dc-link. Regarding those, Wolfspeed 10 kV MOSFET is chosen for each switch in both primary and secondary sides [2].

As shown in Fig. 5, the Wolfspeed 10 kV MOSFET is a three-phase module that each switch has six parallel 10 kV, 15 A dies. On the other hand, the Wolfspeed 10 kV MOSFET can be used as a half-bridge module that each switch has 18 parallel 10 kV, 15 A dies. Since the average primary and secondary currents are 51 A and 92 A, respectively; the Wolfspeed 10 kV MOSFET with three-phase and half-bridge configuration are respectively used for primary and secondary side converters. With respect to Module and topology selections, the required number of the modules for primary and secondary are two for each side.

B. Three-level NPC to two-level DAB control

DAB converters have been used in bidirectional isolated DC-DC converter applications with their advantages of easy control and ZVS ability. The power flowing from one port to another one can be easily controlled by adjusting the phase-shift among the active bridge switching signals as explained as follows:

$$P_{p-s} = \frac{V_p V_s'}{2\pi^2 f_{sw} L_{ps}} \phi(\pi - \phi) \tag{8}$$

where $P_{p\text{-}s}$ is the power; V_p and V_s' are the primary and secondary voltages (reflected to the primary), respectively; f_{sw} is the switching frequency and L_{ps} is leakage inductance, and ϕ is the phase shift angle among the bridges.

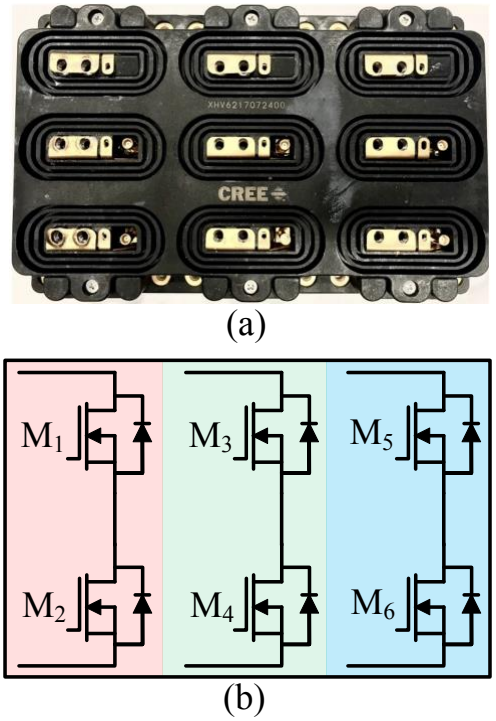

Fig. 5. Latest Wolfspeed 10 kV MOSFET: (a) photograph, (b) switch located inside the module

This is called single-phase shift (SPS) control. It is an easy and effective method to control power. However, for low power conditions, the circulating current becomes higher and therefore reduces the efficiency. To improve efficiency, enhanced modulation strategies have been proposed such as double phase-shift (DPS) and triple phase-shift (TPS) methods. Although these methods provide better efficiency, they increase the complexity. In the TPS method, three variables affect the power flow. This increases the control degree of freedom but also makes difficult to determine the values for each of these variable. The same power level can be achieved by using various control parameters. This feature enables to designers to optimize their control rules to achieve different objectives such as minimum RMS current, maximum power minimum loss, etc. [22],[23].

In this study, to handle the 13kV primary voltage with 10kV switches, a three-level NPC converter is employed as active bridges. In this case, when the TPS method is applied there are five parameters (two duty cycle values for primary active bridge, two duty cycles for the secondary active bridge, and a phase-shift angle) affecting the power flow. The power flowing from primary to the secondary can be written as in (9) where D_{11}, D_{12}, D_{21}, D_{22}, and ϕ are outer and inner phased shift of primary three-level active bridge, outer and inner phased shift of the secondary three-level active bridge, and phase shift angle between bridges, and the L is the primary reflected total leakage inductance of the transformer.

$$P_{av}=\frac{V_p V_s^{'}}{16 f_{sw} L}\left(2D_{11}D_{21}-D_{21}^{\,2}-\phi^2-D_{11}^{\,2}+2D_{11}\phi+2D_{21}\phi+8D_{12}\phi+4D_{22}\phi\right) \quad (9)$$

TABLE II. OPTIMAL MFMV TRANSFORMER CHARACTERISTICS.

	Power, losses, Efficiency, Voltage	Primary Winding	Secondary Winding	Core
Results	*Power=670 KW, V_{in} =13 KV, V_{out} =7.2 kV, μ=99.95%*	*N_P=3*17, AWG#2, ampacity = 132A, insulation = 18Kv; L_p= 64.2 μH*	*N_S=2*15, AWG#1/0, ampacity = 210A, insulation = 10 kV L_s=35.1 μH*	*L_M=1.06 μH, d_{in} = 1.44mm; P_{core}=105 W, P_{copper}=220 W; Core material = Ferrite MnZn BFM8*

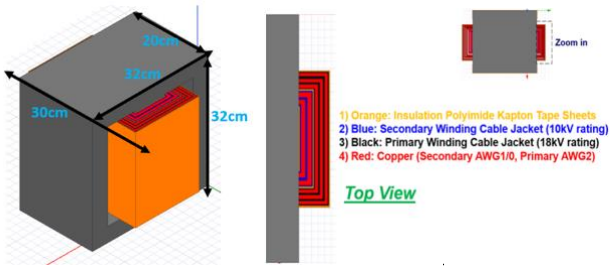

(a) (b)

Fig. 6. (a) 3D view, and (b) Top view of MFT in ANSYS-MAXWELL.

C. Converter cooling system

In order to design a proper cooling system, 10 kV MOSFETs for each primary and secondary sides are modeled in ANSYS-FLUENT, and based on the calculated power loss of each die, a cold plate with a single tube is designed to keep the maximum allowed temperature of the dies below a specified value, which is 80 percent of the maximum junction temperature of the die (140˚C).

V. SIMULATION RESULTS

The first step for designing the SST is the selection of material as well as core type. As discussed in section III, ferrite material is the best option for 20 kHz and 667 kW. Regarding the core mechanical design, a shell-type configuration is chosen thanks to high-efficiency performance, small leakage inductance, and smooth power flow [3]. Then different primary and secondary turns/layers, core dimension, insulation thickness, cooling size, and fan type are considered and modeled in ANSYS-MAXWELL and ICEPAK. Based on each specific parameter, as well as core and winding losses, the temperature distribution is calculated. Among these solutions, the best one is selected that reach has 99.95 % efficiency (Table II). The optimum MFMV transformer obtained out of the optimization process is shown in Fig. 6 (a) and (b). Thanks to the proper design of the cooling system the temperature of the core and winding are limited. Fig 7. shows the temperature distribution and flux density distribution in the final HFMV transformer. As can be seen, the average flux density is 0.35 T, however, the maximum

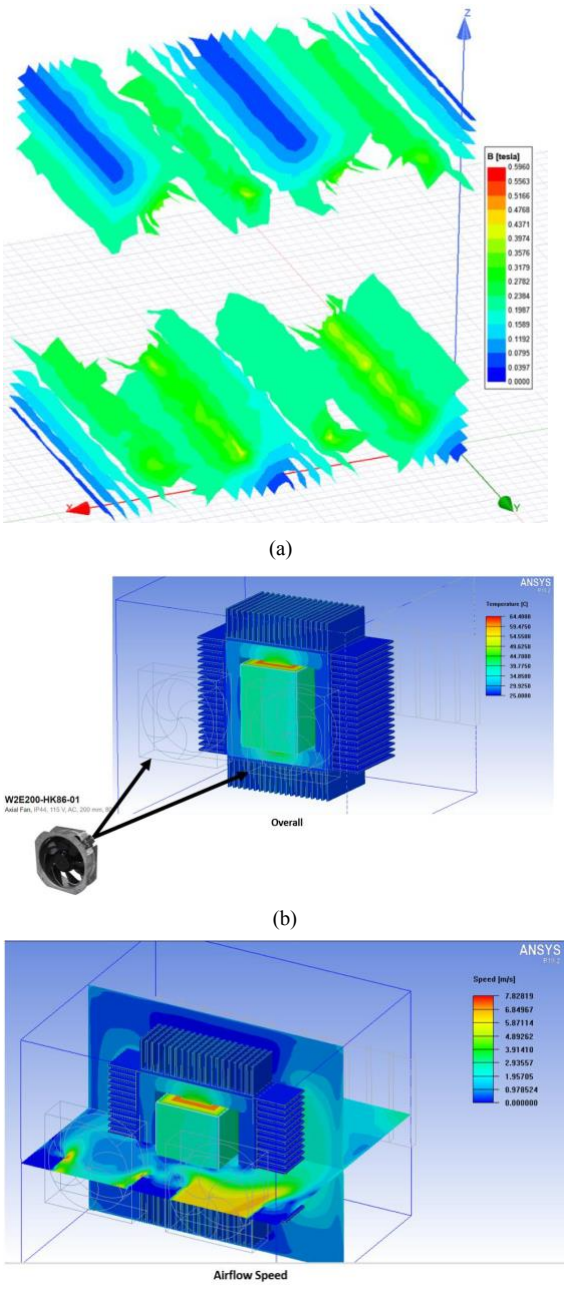

(a) (b) (c)

Fig.7. (a) Flux density distribution (b) temperature distribution, (c) speed distribution.

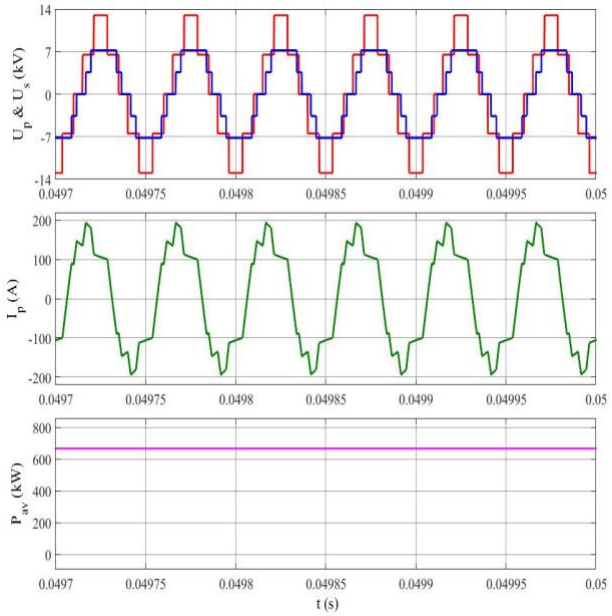

Fig.8. (a) Primary and secondary voltage waveforms, (b) Primary current waveform, (c) The average power transferred from primary to secondary.

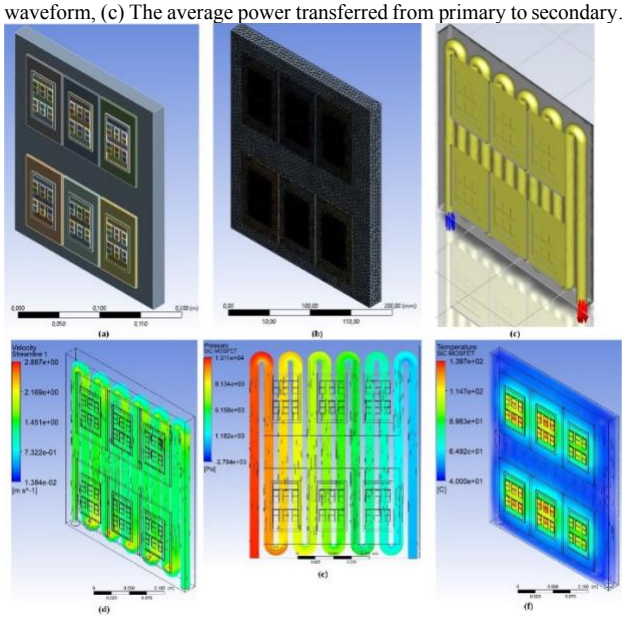

Fig.9. Primary-side converter (a) Two 10 kV MOSFET modules with a cold plate, (b) mesh (c) water channel in the cold plate, (d) water velocity in the channel, (e) Pressure drop in the channel, (f) Temperature on both modules and cold plate

value occurs in the corner, which should not be taken into account. In addition, the maximum temperature of the transformer does not exceed the target temperature which is 70˚.

The optimum values of the primary and secondary duty cycles and phase shift values can be determined to provide 667 kW power from the primary to the secondary side with minimum RMS current or minimum converter loss or any other design objective. The primary winding voltage,

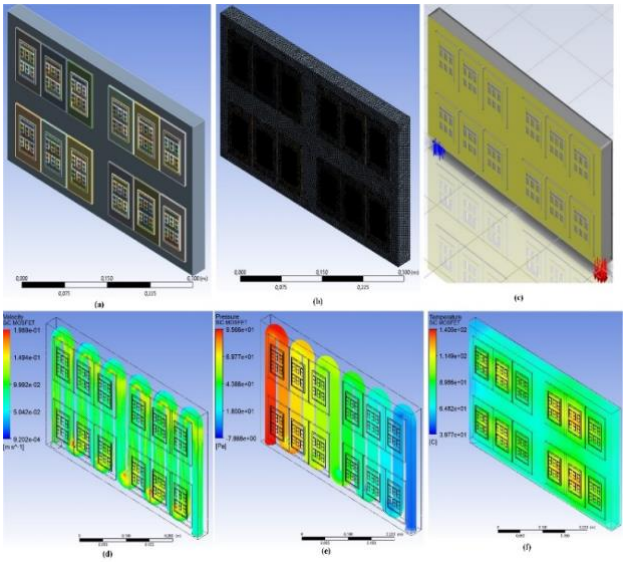

Fig.10. Secondary-side converter (a) Four 10 kV MOSFET modules with a cold plate, (b) mesh (c) water channel in the cold plate, (d) water velocity in the channel, (e) Pressure drop in the channel, (f) Temperature distribution on both modules and cold plate.

the secondary winding voltage, the primary current, and the average load power waveforms are shown in Fig. 8. It is seen that thanks to the three-level NPC topology, 13kV primary voltage can be handled with 10kV power switches.

As the module has six Switches and each one has six dies in parallel, only two and four modules are required for primary and secondary side converters, respectively. Then, based on the simulation results, the RMS current in each dies is measured, Finally, with respect to current amplitude, both conducting and switching power losses are calculated based on Datasheet [2]. These power losses are used for water-cooling system design. The overall primary and secondary converters with a detailed model of 10 kV MOSFET are simulated in ANSYS-FLUENT and shown in Fig. 9 (a) and Fig. 10 (a), respectively.

The first step in designing the water cooling system is the identification of the maximum allowed temperature of 10 kV MOSFET. As mentioned in [2], T_{max} is 175˚, however, for reliability purposes, a derating value of 80% is considered so the target maximum temperature is 140˚. In the next step, as shown in Fig. 9 (b) and Fig. 9 (b) for a different part of the module, an appropriate mesh structure is designed to prevent divergence of solution and aid in approaching to correct result. Due to the dimension of the channel and water flow rate (see Fig. 9 (c) and Fig. 9 (c)), the Reynold number ($Re=\rho.V.D/\mu$) is above 1000, therefore the thermodynamic problem is solved by k-ε turbulence model. Finally, the optimum results that limit maximum junction temperature (140˚) bellows are obtained for primary and secondary converters (see Fig. 9 (d)-(f) and Fig. 10 (d)-(f)).

VI. Conclusion

This paper presents an optimization-based algorithm to reach the highest efficiency in both MFT and converter

parts. In the MFMV transformer, different variables and constraints are considered for optimization purposes. Finally, an optimized configuration of MFT and forced-air cooling gives 99.95%. In the converter part, the 10 kV SiC MOSFET-based NPC converter is modeled in detail in ANSYS-FLUENT. Then, regarding the maximum allowed temperature and power loss of the module, optimal flow rates of the water cooling system for primary and secondary sides are obtained. The simulation results show that with respect to optimum water-cooling design for primary and secondary converters, the junction temperature is limited to 140˚.

ACKNOWLEDGMENT

This material is based upon work supported by the National Science Foundation under Grant No. 1650470. Any opinions, findings, and conclusions or recommendations expressed in this material are those of the author(s) and do not necessarily reflect the views of the National Science Foundation.

REFERENCES

[1] J. W. K. Daniel Rothmund, Thomas Guillod , Dominik Bortis, "99% Efficient 10 kV SiC-Based 7 kV-400 V DC Transformer for Future Data Centers," pp. 753–767, 2019.

[2] B. Passmore *et al.*, "The Next Generation of High Voltage (10 kV) Silicon Carbide Power Modules," in *2016 IEEE 4th Workshop on Wide Bandgap Power Devices and Applications (WiPDA)*, 2016, pp. 1–4.

[3] C. Dimarino *et al.*, "Design and Experimental Validation of a Wire-Bond-Less 10-kV SiC MOSFET Power Module," *IEEE J. Emerg. Sel. Top. Power Electron.*, vol. 8, no. 1, pp. 381–394, 2020.

[4] T. Liu, X. Yang, W. Chen, Y. Li, Y. Xuan, and L. Huang, "Design and Implementation of High Efficiency Control Scheme of Dual Active Bridge Based 10 kV / 1 MW Solid State Transformer for PV Application," *IEEE Trans. Power Electron.*, vol. 34, no. 5, pp. 4223–4238, 2019.

[5] P. Zumel *et al.*, "Modular Dual-Active Bridge Converter Architecture," *IEEE Trans. Ind. Appl.*, vol. 52, no. 3, pp. 2444–2455, 2016.

[6] A. Q. Huang, Q. Zhu, L. Wang, and L. Zhang, "15 kV SiC MOSFET : An Enabling Technology for Medium Voltage Solid State Transformers," *CPSS Trans. POWER Electron. Appl.*, vol. 2, no. 2, pp. 118–130, 2017.

[7] A. K. Tripathi *et al.*, "Design Considerations of a 15-kV SiC IGBT-Based Isolated DC – DC Converter," *IEEE Trans. Ind. Appl.*, vol. 51, no. 4, pp. 3284–3294, 2015.

[8] S. Kenzelmann, A. Rufer, D. Dujic, S. Member, F. Canales, and Y. Rˆ, "Isolated DC / DC Structure Based on Modular Multilevel Converter," *IEEE Trans. Power Electron.*, vol. 30, no. 1, pp. 89–98, 2015.

[9] X. Zhao *et al.*, "DC Solid State Transformer Based on Three-Level Power Module for Interconnecting MV and LV DC Distribution Systems," *IEEE Trans. Power Electron.*, vol. 36, no. 2, pp. 1563–1577, 2021.

[10] P. Liu, C. Chen, S. Duan, and W. Zhu, "Dual Phase-Shifted Modulation Strategy for the Three-Level Dual Active Bridge," *IEEE Trans. Ind. Electron.*, vol. 64, no. 10, pp. 7819–7830, 2017.

[11] Marko Mogorovic and Drazen Dujic, "100 kW, 10 kHz Medium-Frequency Transformer Design Optimization and Experimental Verification." pp. 1696–1708, 2019.

[12] T. Guillod *et al.*, "Dielectric Losses in Dry-Type Insulation of Medium-Voltage Power Electronic Converters," *IEEE J. Emerg. Sel. Top. Power Electron.*, vol. 8, no. 3, pp. 2716–2732, 2020.

[13] H. P. Transformers *et al.*, "Analytical Design Methodology for Litz-Wired High-Frequency Power Transformers," *IEEE Trans. Ind. Electron.*, vol. 62, no. 4, pp. 2103–2113, 2015.

[14] X. Yu, J. Su, J. Lai, S. Guo, and S. Member, "Analytical Optimization of Nonsaturated Thermally Limited High-Frequency Transformer / Inductor Design Considering Discreteness of Design Variables," *IEEE Trans. Power Electron.*, vol. 35, no. 6, pp. 6231–6250, 2020.

[15] M. K. Bahmani, M Amin, Torbjorn Thiringer, "Design Methodology and Optimization of a Medium-Frequency Transformer for High-Power DC – DC Applications," *IEEE Trans. Ind. Appl.*, vol. 52, no. 5, pp. 4225–4233, 2016.

[16] M. Leibl, G. Ortiz, and J. W. Kolar, "Design and Experimental Analysis of a Medium-Frequency Transformer for Solid-State Transformer Applications," *IEEE J. Emerg. Sel. Top. Power Electron.*, vol. 5, no. 1, pp. 110–123, 2017.

[17] S. Zhao, S. Member, Q. Li, and F. C. Lee, "High-Frequency Transformer Design for Modular Power Conversion From Medium-Voltage AC to 400 VDC," *IEEE Trans. Power Electron.*, vol. 33, no. 9, pp. 7545–7557, 2018.

[18] M. Mogorovic, D. Dujic, and S. Member, "Sensitivity Analysis of Medium-Frequency Transformer Designs for Solid-State Transformers," *IEEE Trans. Power Electron.*, vol. 34, no. 9, pp. 8356–8367, 2019.

[19] C. Bin, "Design optimisation of an inductor-integrated MF transformer for a high-power isolated dual-active-bridge DC – DC converter," *IET Power Electron.*, pp. 1–11, 2019.

[20] Y. Du, S. Baek, S. Bhattacharya, A. Q. Huang, and A. Arnon, "High-voltage High-frequency Transformer Design for a 7 . 2kV to 120V / 240V 20kVA Solid State Transformer," in *Annual Conference on IEEE Industrial Electronics Society*, 2010, pp. 493–498.

[21] Y. Liu *et al.*, "Quarter-Turn Transformer Design and Optimization for High Power Density 1-MHz LLC Resonant Converter," *IEEE Trans. Ind. Electron.*, vol. 67, no. 2, pp. 1580–1591, 2020.

[22] G. Jean-pierre, N. Altin, A. El Shafei, and A. Nasiri, "Efficiency Optimization of Dual Active Bridge DC – DC Converter with Triple Phase-Shift Control," in *IEEE Energy Conversion Congress and Exposition (ECCE)*, 2020, pp. 1217–1222.

[23] G. Jean-pierre, M. Khayamy, N. Altin, A. El Shafei, and A. Nasiri, "A Triple Phase-Shift Based Control Method for RMS Current Minimization and Power Sharing Control of Input-Series Output-Parallel Dual Active Bridge Converter," in *IEEE Transportation Electrification Conference & Expo (ITEC)*, 2020, pp. 550–555.